# DRONE POWER LINE TRACKING AND AVOIDANCE

---

**PROJECT REPORT**

**Submitted in Partial Fulfillment of**

**the Requirements for**

**the Degree of**

**MASTER OF SCIENCE (Mechatronics and Robotics)**

**at the**

**NEW YORK UNIVERSITY**
**TANDON SCHOOL OF ENGINEERING**

**by**

**Alex Colbourn**

**May 2019**

# DRONE POWER LINE TRACKING AND AVOIDANCE

## PROJECT REPORT

**Submitted in Partial Fulfillment of**

**the Requirements for**

**the Degree of**

## MASTER OF SCIENCE (Mechatronics and Robotics)

**at the**

## NEW YORK UNIVERSITY
## TANDON SCHOOL OF ENGINEERING

**by**

**Alex Colbourn**

**May 2019**

Approved:

Advisor Signature

Date

Department Chair Signature

Date

University ID: **N17638164**
Net ID: **ac7012**

# ABSTRACT

## DRONE POWER LINE TRACKING AND AVOIDANCE

**by**

**Alex Colbourn**

**Advisor: Professor Maurizio Porfiri, Ph.D.**

**Co-Advisors: Frank Vallese, Ph.D. and Jeffrey Laut, Ph.D.**

**Submitted in Partial Fulfillment of the Requirements for**

**the Degree of Master of Science (Mechatronics and Robotics)**

**May 2019**

Power lines pose a significant threat to virtually all aircraft. They are extremely difficult for human and autonomous systems to detect and are a frequent source of fatal or catastrophic accidents. In addition, dangerous and costly line inspections need to be performed regularly by power companies. This paper investigates the feasibility of using the substantial electric and magnetic fields surrounding power lines as a means for avoidance and automated line inspection. It investigates the types of fields generated by the lines, various methods for measuring them, and potential ways to commercialize this technology. A proof-of-concept test setup was created and used to conduct experiments near a transmission line. A simulated magnetic field model was then verified with this real-world data. Both the electric and magnetic fields are crucial to this design. The results show the feasibility of the magnetic field portion of this method and address ongoing efforts to do the same for the electric field.

## Table of Contents



## List of Figures

## 1. Introduction

In recent years, the prevalence of drones throughout the world has grown at an incredible rate. A Goldman Sachs analysis predicts that between now and 2020, drones will represent a $100 billion market opportunity [1]. While this market will be primarily dominated by defense spending ($70 billion), the consumer and commercial markets are finding ever-expanding new uses for drones including construction, agriculture, insurance, journalism, and photography to name a few. The consumer drone market alone is expected to have 7.8 million drone shipments by 2020 [1]. Unfortunately, this rapidly growing volume of drones brings with it an equally fast paced growth of safety concerns. Amazing breakthroughs have been made on this front recently including vision-based obstacle avoidance and geofencing to automatically prevent drones from flying within hazardous restricted airspace. The problem of avoiding power lines, however, has yet to be successfully addressed despite being a significant threat to nearly the entire global drone market.

Power lines pose several unique challenging problems for drones and are widespread throughout the world. First, they happen to be at a very common height for drone flight paths. In addition, they are too narrow to be easily resolved by cameras, making them almost impossible to see for both pilot-operated and autonomous systems. At night, they are essentially invisible to vision-based avoidance sensors. To make matters worse, the electromagnetic fields they emit are so strong that even if a drone does not directly strike the line, merely being in the vicinity of a line can lead to a crash. Drone control systems often rely on GPS and magnetic readings that are significantly impacted by power line noise which often leads to a complete loss of control [9].

In addition to power line avoidance, there is a significant interest in utilizing the electromagnetic fields to track the power lines and perform inspections. The most obvious uses being military, power companies, and disaster recovery such as

quickly analyzing the power grid after a hurricane. To our surprise, we discovered that it is still incredibly common for power companies to perform line inspections with helicopters hired for several thousand dollars an hour. The cost savings of switching to automated drone inspections are obvious but, more importantly, the increased safety of an automated system has helped motivate our research. Sadly, just a few weeks before this paper was written, two workers were killed in a helicopter crash while inspecting a line [10].

The primary goal of this research is to assess the feasibility of using electromagnetic fields to both avoid and follow power lines. The following sections describe the ongoing validation of this technology and potential avenues for commercialization based on our current findings.

## 2. Background Overview

In order to understand the focus of our research, a very brief overview of electromagnetics and common power line parameters is necessary. Power lines radiate primarily two types of fields that are of interest to us, electric fields and magnetic fields. Electric fields are present any time the line is energized, but magnetic fields are only generated when current is flowing in the line. This is a critical distinction because if no or little current is flowing, the magnetic field is rendered completely useless for detecting a line. The electric field, on the other hand, is always present if the line has voltage, but it is notoriously complicated to measure and extremely vulnerable to distortions from nearly everything around it. The proposed technology leverages both fields to reduce the chance of errors that would arise from relying on only one measurement source. By combining both and their derivates, a much more robust detection algorithm can be created. In addition, by taking the cross products of each field, the Poynting vector can be derived which points nearly parallel to the direction of the power line. This vector is the key parameter required for the power line tracking version of our proposed product [2].

The fields generated by power lines can be divided into near and far field regions. The boundary between these regions is defined by the electromagnetic wavelengths, and at power line frequencies these wavelengths are thousands of kilometers. For this reason, our research focuses exclusively on the near field. In the far field, coupled electromagnetic effects such as wave propagation dominate, but in the near field they are negligible and can thus be ignored. Instead, we treat the electric and magnetic fields as independent quasistatic entities [3].

We are measuring 60 Hz, 3-phase power lines. For simplicity, we assume each wire is an infinite, straight conductor, with all conductors running in parallel such that the electric and magnetic fields can be modeled in just two dimensions. In reality, there is a small component in the direction of the wire caused by factors like wire sag and branch wires, but they are expected to be negligible compared to the other two axes. Worth noting is that the electric field is much more prone to distortions by things like transmission towers, so it will typically have more 3-d effects than the magnetic field, but this is not accounted for in our model [3]. Our coordinate axis can be seen in Figure 1 below. When looking at a transmission tower, the positive X direction is to the right, the positive Y towards the tower, and positive Z is towards the sky. For the ideal case, the magnetic field components in the X and Z directions can be found by the Biot-Savart Law as follows:

$$H_X = -\frac{1}{2\pi}\sum_n I_n \frac{Z - Z_n}{(X - X_n)^2 + (Z - Z_n)^2} \quad (1)$$

$$H_Z = \frac{1}{2\pi}\sum_n I_n \frac{X - X_n}{(X - X_n)^2 + (Z - Z_n)^2} \quad (2)$$

Where $I_n$ is the instantaneous current on the $n^{th}$ line, $X_n$ and $Z_n$ are the horizontal offset and height of the lines, and X and Z are the horizontal offset and height of the measurement point [3].

The equations for the X and Z electric field components are as follows:

$$E_X = \frac{1}{2\pi\epsilon_0}\sum_n \lambda_n\left(\frac{X - X_n}{(X - X_n)^2 + (Z - Z_n)^2} - \frac{X - X_n}{(X - X_n)^2 + (Z + Z_n)^2}\right) \quad (3)$$

$$E_Z = \frac{1}{2\pi\epsilon_0}\sum_n \lambda_n\left(\frac{Z - Z_n}{(X - X_n)^2 + (Z - Z_n)^2} - \frac{Z + Z_n}{(X - X_n)^2 + (Z + Z_n)^2}\right) \quad (4)$$

Where $\lambda_n$ is the linear charge density, $\epsilon_0$ is the permittivity of free space, $X_n$ and $Z_n$ are the horizontal offset and height of the lines, and X and Z are the horizontal offset and height of the measurement point. This is a very brief overview of a model based heavily on software simulations done by the Army Research Lab, for more detailed information see reference [3].

The magnetic field can be simplified visually as rings around the power line. The electric field can be visualized as emanating radially in every direction from the line and shorting out to Earth. The Earth is treated as a perfectly conducting infinite ground plane and is capacitively coupled to the power lines which causes the electric field to bend towards it [3]. Figure 1 below depicts my coworkers simplified visual for the ideal cases outlined above, the magnetic field is in grey and electric field in blue.

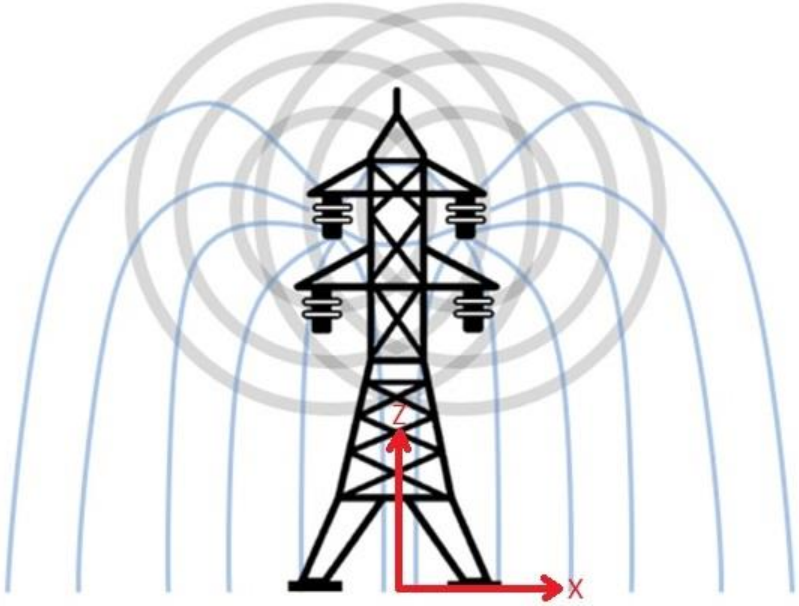


**Figure 1: Visualization of Electric and Magnetic Fields and Axis Definition**

The next critical component to understanding the fields are the operating principles of the power grid itself. Typical power lines globally transmit three phase power. Three phase power is a method of transmitting AC power over three wires that are synchronized to be 120 degrees out of phase from each other. In the United States, the standard is 60 Hz AC, but 50 Hz AC is equally popular around the world. DC power is also growing increasingly popular, due in large part to China and the rise of renewable energy. Our final system will need to account for all these possibilities, but we will initially be targeting the 60 Hz AC United States market. An interesting side note is that aircraft typically use 400 Hz systems which may make it possible to isolate them with our system as well and add aircraft avoidance to our core technology [4]. The market for this feature is considerable as collisions with manned aircraft are the primary safety concern facing the industry. As equations 1 - 4 outline above, the generated fields are superpositions of each power line present in the system. Therefore, the specific geometry of a set of lines will determine its specific field. In addition to the standard configuration of one set of three phase power, it is very common for other configurations to exist such as towers carrying two full sets of three phase power, or a distribution line carrying just 2 phases to an individual house, for example. Regardless of configuration, the resulting fields are always the superpositions of the individual lines.

Further impacting the fields are harmonics primarily generated by the various loads connected to the line such as motors, rectifiers, and inverters. The odd harmonics at 180 Hz and 300 Hz tend to dominate the fields because the 120-degree phase shift between the lines causes them to add together as shown in Figure 2 below. The even harmonics can still be significant depending on a variety of factors, however, so our system focuses on the first five harmonics (60 Hz, 120 Hz, 180 Hz, 240 Hz, 300 Hz) [4]. Once again, these harmonics are all added together by superposition. The resulting fields are thus complex waveforms composed of the combination of all these factors, creating unique and ever-changing footprints for

every power line. Our team is investigating whether it is possible to autonomously infer the configuration of a tower from this unique harmonic footprint.

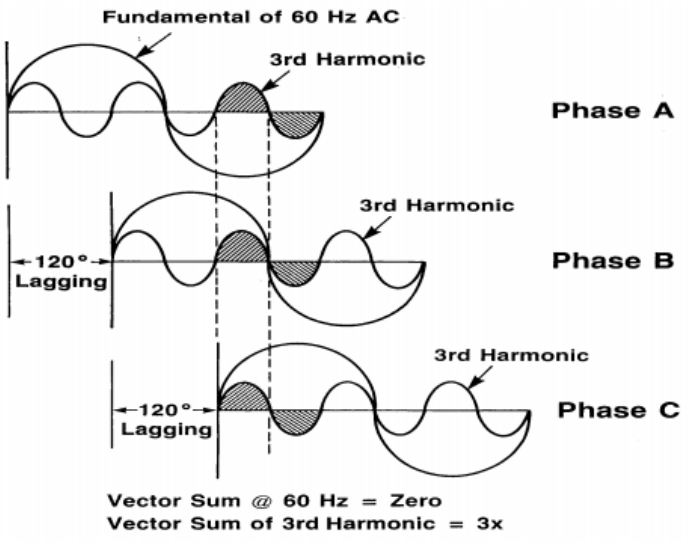


**Figure 2: Visualization of Additive 3rd Harmonic for 3-phase power [4]**

## 3. Sensors

Much of the effort on this project has been the narrowing down of potential equipment for commercialization. The primary factors involved were size, weight, cost, repeatability, and range. An extensive array of readily available magnetometers has been narrowed down to two primary sensor choices/types. A summary and comparison of each is outlined below.

The first is the Honeywell HMC2003 which is a 3-axis magneto-resistive sensor. This operates on the principle that the resistivity of a current carrying ferromagnetic material changes due to a magnetic field. When a magnetic field passes through a flat plate of this material, the resulting change in current can be measured and correlated to the corresponding magnetic field strength. This effect is highly dependent on the angle of the field passing through the plate. It is maximized perpendicular to the plate and has no effect if the field is parallel to the plate. By placing 3 of these plates orthogonally, the three-dimensional field is obtained [5].

This sensor has a resolution of 40 microGauss, +/- 2 Gauss dynamic range, and costs $344. Important to note is that the individual axes can be purchased separately for a combined cost of roughly $35. After adding the rest of the needed circuitry, the actual cost will likely be below $45.

The Trifield TF2 is the other primary choice and was picked mainly for its low cost. Unlike the Honeywell, it is not intended as a sensor add-on. It is a standalone meter with an inbuilt screen and has no outputs for measurements by other means. It was picked for the purpose of reverse engineering its extremely cheap magnetic and electric field sensors and creating a similar design based on these operating principles. The magnetic field component uses three ferrite-core coils pointing in the X, Y, and Z directions to compute one combined total field reading. Like the magnetoresistive sensor, a coil is only sensitive to the flux perpendicular to its main axis, so it uses three mutually perpendicular coils. It works on the principle that a magnetic flux passing through a coil of wire induces a current. This effect can be increased by using a larger coil area or introducing more loops. A ferromagnetic core placed in the center of the coils acts as a flux concentrator and allows the system to be miniaturized [6]. The Trifield's magnetic resolution is 0.1 milliGauss, it has a 100 milliGauss range, and costs $168. The inductive coils it uses, however, can be purchased in bulk for roughly 30 cents. After adding its additional circuitry, the total cost of this option is likely less than $5.

Comparing these sensors, there are some major tradeoffs to consider. Their footprints and weight are roughly similar, and both are small enough to be used in an actual product. The Honeywell provides a polished, calibrated solution that is designed specifically for Aerospace. It has significantly better resolution and range but a dramatically higher price. It is without a doubt the winner in terms of time to a functional prototype. The Trifield method is inferior in every way except for cost. It will take time to develop its circuitry and calibration. In addition, as of this report we have only been able to test these sensors at ground level. They both performed well at this height where fields were relatively low but depending on how close

inspection drones need to get, the Honeywell's extended range may become a critical factor. For the immediate future, both methods will continue to be tested side by side until we have the market research and data to make a final decision.

Unfortunately, the plethora of options available for the magnetic field is in stark contrast to the complete void of options found in the electric field market. Almost all existing solutions require elaborate setups, cost much more than the average drone, and are roughly the same size as the drone itself rendering them useless. Months of research has led to the conclusion that a custom sensor will need to be developed. Numerous small experiments have been conducted towards this end with little in the way of meaningful results, but two possible methodologies are finally starting to emerge. The first is the original plan of reverse engineering the Trifield. Both the working principle and accuracy of this meter are still a source of debate, however. What we do know is that the sensor itself is simply a flat, rectangular copper plate with a single wire soldered to it. What happens from there is mostly speculation at this point, so our findings will be omitted from this paper until confirmed. What can be commented on, however, is the extremely low cost, decent performance, and size. A three-axis system could potentially be made with three orthogonal copper plates and associated amplifiers for just a few dollars. The plate size and weight are larger than ideal, but within a feasible range and can perhaps be further reduced. The design is tested and known to work for at least ball park estimates, but in general this meter is not known for the extreme accuracy of its e-field measurements (it sells primarily based on its magnetic reading accuracy).

The primary type of electric field sensor we are now investigating is called a free-body meter. In this design, two parallel copper plates are spaced a small distance apart and a small alternating electric potential is induced between them by a varying electric field. This signal is then amplified and calibrated to a known field [7]. A three-axis implementation would simply be a cube with 6 plates. This design has appeared many times with slight variations in our literature review and is the

most promising path forward. The circuit can be seen in Figure 3 below. We recently built a prototype of this circuit and first impressions were very promising. 60 Hz and the expected harmonics were all clearly detected and moving a live wire towards and away from the plates yielded very similar corresponding changes in detected amplitude. The main challenge going forward will no doubt be proper calibration and shielding.

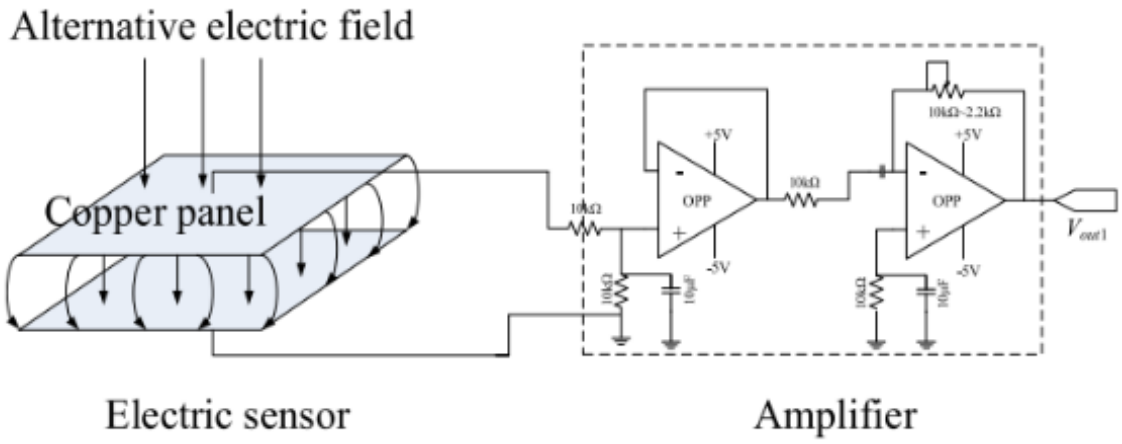


**Figure 3: Free-body Electric Field Meter Circuit [7]**

The paradox of electric field sensor design is that it's both extremely difficult to correctly detect the field, and almost impossible not to detect it. In previous experiments we have seen that when we disconnected our sensor, we were still reading values of the same order of magnitude. This was due to the wiring acting like an omnidirectional e-field antenna itself. It is even possible to detect the electric field by reading an empty channel with absolutely nothing connected to it as electrical grid noise is seemingly omnipresent. Sorting out the differences between actual sensor readings and noise is particularly challenging in our case because there is no discernable difference between the two. No amount of signal processing will help as the noise itself is what we are measuring. This makes proper shielding critical as it is the only tool left to combat noise. In addition, small changes in the room have big impacts on readings as fields from different angles got blocked or distorted. For example, taking a reading with the Trifield while

holding it will give completely different results than a measurement in the exact same location but attached to a mount. Precision meters go to painstaking lengths to reduce errors like this including running fiber optic cable to a meter placed on an isolated tripod several feet from any other electronics. We are attempting to deal with this problem through wire shielding, Faraday cages, and location. We will likely need to calibrate our sensor in a large open space such as a park where noise is as minimal as possible. The Army Research Lab has built an isolated room specifically for this purpose and offered to help us calibrate when we are ready. It can produce extremely accurate known fields in a virtually noise free environment.

## 4. Experimental Setup/Method

The heart of our experimental setup is a National Instruments CompactDAQ cDAQ-9191 chassis. Inside of it is an NI-9202 16 channel, 10kS/s, +/- 10 Volt, 24-bit analog input card. This setup is a near perfect solution for our prototyping requirements. It is easily powered from a battery, allowing us to gather data in the field. It supports wireless data streaming, allowing us to send it up in a cherry picker with inspection workers to gather data extremely close to the lines. At 10kS/s we can resolve frequencies up to 5000 Hz, and with it's extremely high 24-bit resolution we can quickly prototype sensor designs without any extra amplification. In addition, with 16 inputs we can test up to 5 entire 3-axis sensors simultaneously for comparison.

A data logging program was written in LabVIEW to perform a variety of tasks. It has two primary modes, a live view that represents what the drone is currently seeing and a recording mode that automates as much of the data gathering process as possible. Recording mode has inputs for position relative to the power line and manual Trifield measurements. All data is saved as raw voltages to retain flexibility so various processing algorithms can be tested later. On startup, it runs an automated calibration of the Honeywell sensor over a serial connection. It does

this by generating a large magnetic pulse on each axis of the sensor to reset its magnetization and ensure the full range of the sensor is utilized.

Over time, a set of standardized processing subroutines were created and optimized for our specific purpose. Everything was coded as generically as possible to allow future sensors and processing to be added quickly. All data is recorded at a sample rate of 2000 SPS. We are primarily interested in recording up to 300 Hz, so Nyquist's Theorem dictates a minimum of 600 SPS. 2000 SPS gives a good safety factor and was found to be an optimal value to reduce the chance of data loss when wirelessly streaming many channels. All data is first scaled from raw voltages into appropriate units for the given sensor. Then, it passes through a high pass filter with a 20 Hz cut-off point and low pass filter with a 400 Hz cutoff point. Both filters are 3rd order infinite impulse response Butterworth filters chosen primarily for speed. Next the amplitudes are measured in units of milliGauss RMS. The three components of the magnetic field are then combined to calculate the total field by the following equation [2]:

$$|H| = \sqrt{|H_x|^2 + \left|H_y\right|^2 + |H_z|^2} \tag{5}$$

Next, a Fast Fourier Transform with a Hanning window is applied to each channel to measure the RMS values. After a thorough literature review, it became evident that no clear standard exists for this type of magnetic FFT. I therefore defined our standard in units of dBmG RMS. To do this, the results of the FFT were scaled into dB relative to a reference of 1 milliGauss by the following formula [8]:

$$H\ (dbmG) = 20log_{10}\frac{X(mG)}{1(mG)} \tag{6}$$

Each channel is then graphed on a Spectrogram to view frequency changes over time. In addition, a program was developed to pick out the amplitudes of the first five harmonics from each channel. It finds the amplitudes of each harmonic (+/-

3% of the frequency) and again converts to units of dBmG RMS. A threshold is then used to trigger a Boolean indicator of whether each frequency is present. A screenshot demonstrating the overview of the magnetic field readings is provided in Figure 4 below.

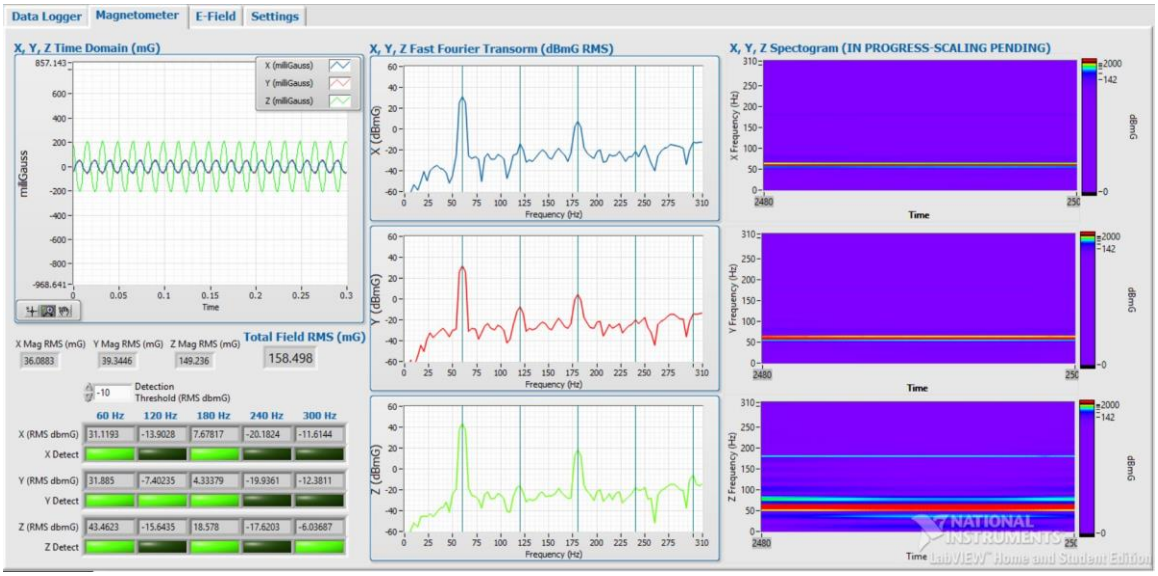


**Figure 4: LabVIEW Program Example of Magnetometer Processing**

A separate data processing program was then created to analyze the collected data sets. It reads from the raw data files and processes everything similarly to the live data program. The primary difference is that it calculates the averages over a data set. With the live data program, everything is near instantaneous so what you see on the screen is what is currently happening. When processing a large stored data file, the question becomes which points in time to analyze. If for example, the sensor is taken from far away and moved towards a power line over the course of a minute, specifying a time interval over which to compute the averages becomes important. This program is still under development, but in its current form it calculates the key average parameters over a full data set and outputs a summary excel file. Selectable timeframes are being added.

## 5. Results

Our primary test had three main goals: verification of our simulated magnetic field model, verification of our magnetic sensor choices, and an estimate of maximum detection distance from a power line with our equipment. The test was performed in an open parking lot at North Hempstead Park Beach. A transmission line with two sets of three phase power was tested. Line voltages and currents were unknown. Starting directly under the line, data was gathered in 3-meter increments moving perpendicular to the line in the X direction as defined in Figure 1. The Honeywell sensor was mounted on top of a 1-meter tripod built out of PVC to prevent distortions in the fields. At each point, data was logged from both the Honeywell and Trifield.


**Figure 5: Overview of North Hempstead Park Beach Location, Transmission Line is Shown Highlighted in Yellow**

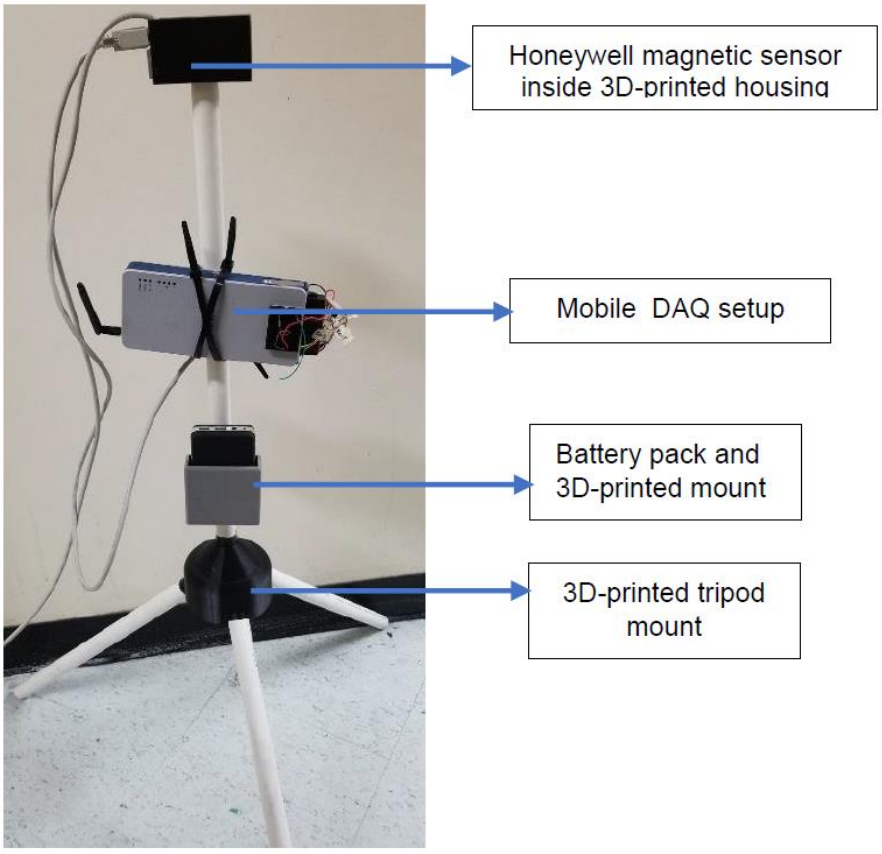


**Figure 6: Overview of Experimental Setup**

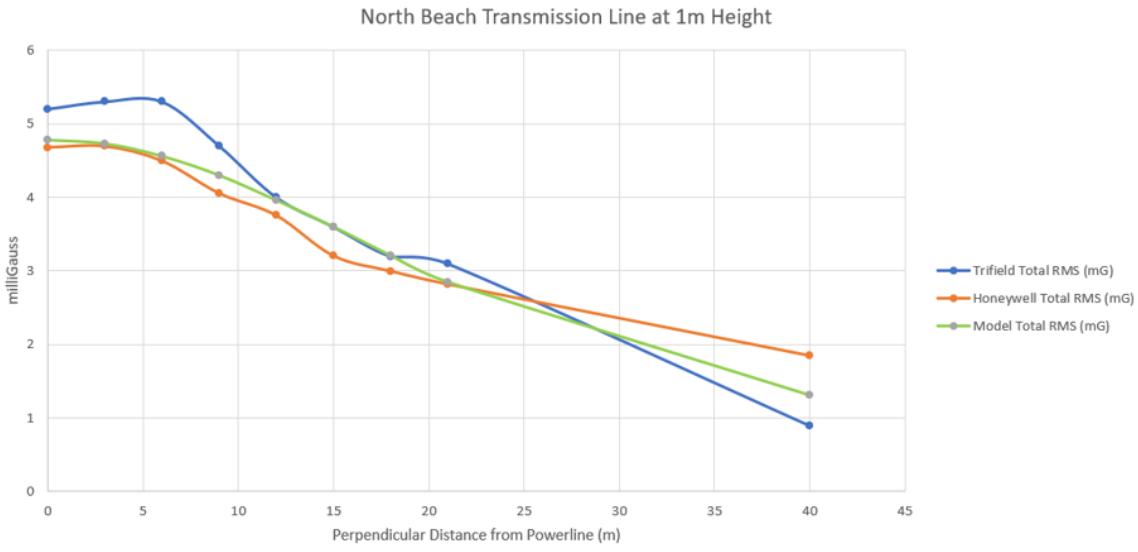


**Figure 7: Comparison of Real-World Magnetic Data and Model**

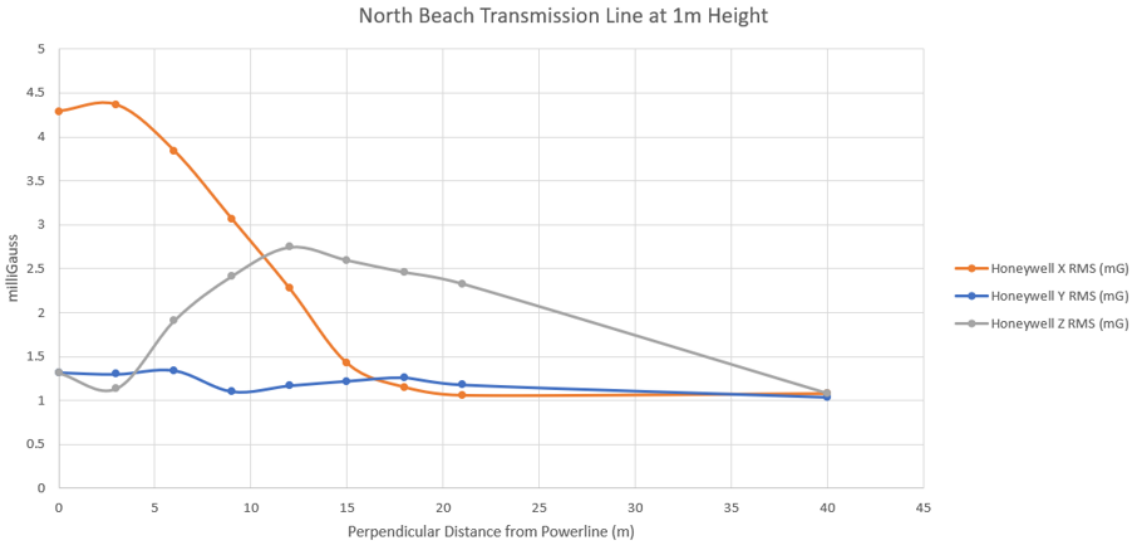


**Figure 8: Three-Axis Honeywell Magnetometer Transmission Line Data**

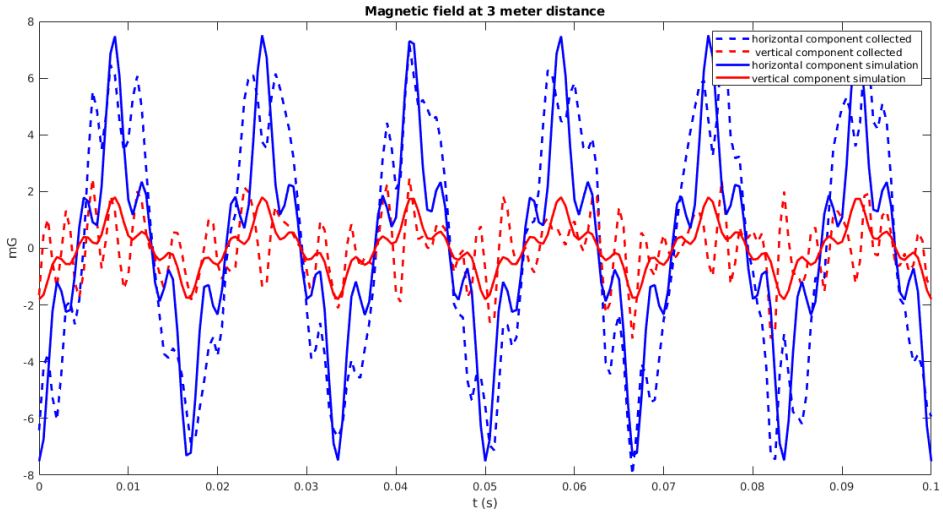


**Figure 9: Comparison of Honeywell X and Z Axes to Simulated Model**

We have also begun preliminary testing on several drones to begin developing a sense of the magnitudes and frequencies of noise they emit. This testing was performed by strapping the drones directly to the top of the Honeywell/Tripod to approximate the sensor being rigidly attached to the center of the body of the drone. The motors were then actuated over 10 seconds at varying velocities while data was recorded. Three drones were tested in this way, a miniature brushless

motor drone, a miniature brushed motor drone, and a high-power brushless racer drone. All testing was done in the middle of an empty classroom, a data set of the classroom with no drone was also captured. This data is still being analyzed but an overview of the Fast Fourier Transforms for each axis of the Honeywell is shown below for each test.

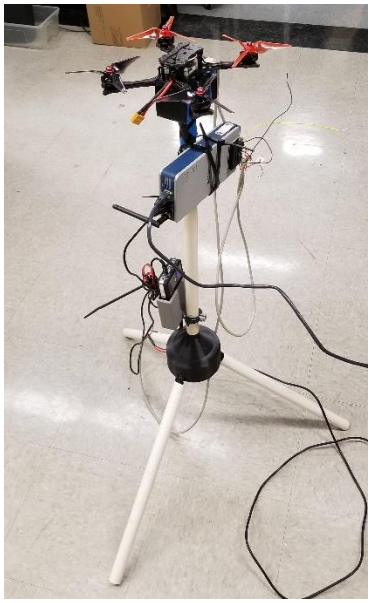

**Figure 10: Drone Test Setup**

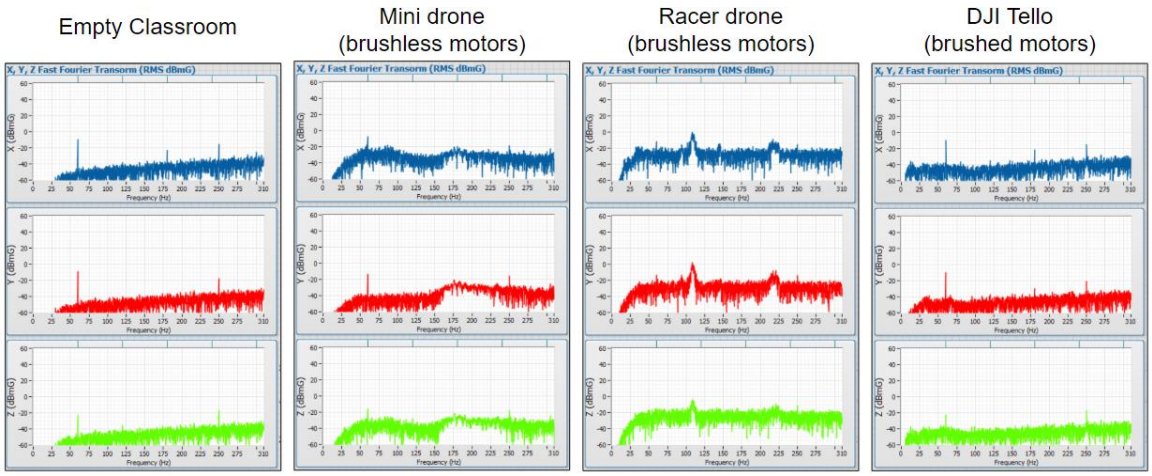


**Figure 11: Preliminary Overview of Magnetic Noise Data from 3 Drones**

## 6. Discussion

Many important conclusions can be drawn from this initial data. Most importantly is that the magnetic fields are behaving very close to the expected results as outlined in section 2. Figure 7 demonstrates a very similar trend between the Honeywell, Trifield, and simulated model. All have slight offsets from each other, however, which can be accounted for by several factors. First are the error bounds of each sensor, the Trifield is accurate to +/- 4% while the Honeywell is accurate to +/- 2%. The bandwidths are also significantly different, the Trifield measures from 40 Hz to 100 kHz while we filter the Honeywell between 40 Hz and 400 Hz. The Trifield is also presumably much more resistant to noise because it is purpose built for this scenario and it has a significantly smaller form factor for noise to penetrate. The model was matched by manually guessing the line voltages and currents, but for a true comparison these values must be known. This brings up an important aspect of our design which is that exact values are not critical. In a real-world scenario we will never know the exact voltage and current on a line and our present objectives don't require reporting field strengths. Unlike most meters on the market, this means extreme accuracy is irrelevant in our case. What matters for us is purely consistency and relative levels. This fact will allow us significant cost savings in calibration time. This test demonstrated that all three methods trended in the same predictable way, simultaneously verifying all of them.

Figure 9 attempts a further verification of the model by overlaying the X and Z axes of the real-world data and simulated data on top of each other in the time domain. After aligning the waveforms and estimating line parameters, they ended up looking somewhat similar, however, further work on the model is needed to better capture the nonlinearities of the acquired data. Overall amplitudes and relative levels of the 60 Hz components in both axes matched as expected. The harmonics show up in a similar pattern but again, as the harmonics primarily depend on the load of the line, getting them to match better is still under development.

Figure 8 is a verification of the directionality of the fields. As predicted in the model, the field in the X direction was highest directly under the line. As we moved perpendicular to the line, the field in the X direction slowly decreased while the Z direction increased proportionately as the magnetic field passed through the sensor at a different angle. The field in the Y direction stayed roughly constant as expected, but interestingly was offset from the expected value of 0 by an average of 1.2 mG. There are several possible explanations for this as discussed in section 2, but there are many indications that this is mostly noise from the wiring. While the wiring we used technically had a shield, it was of very low-quality and the lengths were long to try and prevent picking up noise from the DAQ. Furthermore, at 40 meters every axis read almost the exact same offset value as the Y direction. This makes its highly likely that the wiring was acting as an antenna and simply picking up the electric field.

A key number that will dictate virtually all decisions going forward is the detection distance from the line. Sensor selection and therefore the entire hardware design is fundamentally tied to maximizing this distance. This distance will ultimately dictate the types of drones our system can be used on due to the reaction times of various UAV's. For example, a quadcopter that can stop on a dime may require only a few meters advance notice to avoid a line, but a high-speed fixed wing drone will require a significantly earlier warning to avoid a crash. Much more testing is needed to verify this number, but a preliminary rough magnetic field distance estimate can be inferred for the North Beach transmission line. The limitation once again comes down to the extreme system noise, but it is clear from Figures 7 and 8 that an actual magnetic field is being detected at 21 meters. By taking the Y axis's largest reading as a worst-case noise floor of 1.34 mG (or 1.85 mG for the combined total field), both the Honeywell and Trifield are clearly detecting well above that at 21 meters. This places the detection distance someplace between 21 and 40 meters where the signals fade completely into noise. Steps to improve shielding are underway to further verify this result.

While the drone data in Figure 11 is still being analyzed, one possible important result can be drawn simply from the spectrum graphs: brushed motors appear to have significantly less magnetic noise at power line frequencies than brushless motors. If this turns out to be true, it may allow for a fully functioning demonstration prototype to be created much sooner than expected. Ultimately, we will need to deal with brushless motors as they are much more common, but I suspect a flying prototype will have much more utility in an investment meeting than noise reduction plots.

## 7. Minimum Viable Product (MVP)

As with any startup, creating an MVP early is critical to survival so here is my recommendation for a possible MVP. I believe a sensor add-on that focuses primarily on avoidance for quadcopters is the fastest path forward. The functionality would be incredibly simple; when our system detects a power line it sends a warning signal to the drone.

Using that signal, individual hobbyists or manufacturers could then easily program any action they want independently of our system. It could simply be a warning, or even better take advantage of most modern drones built in function to hover in place. The user would then be able to unlock the drone through software and fly away when they have identified the direction of the power line. To help with this, the software could allow the drone to spin in place while locked so the camera can be used to spot the power line. Another possibility is simply reversing course a few steps (to what was presumably a safe location) and then hovering in place.

This method has numerous advantages. First is time; we are right around the corner from being able to do this right now. Being first to market even with a very basic product has obvious advantages and will allow us to start getting feedback. This would be a monumental simplification of the problem while achieving the same crash avoidance results. It would require user input, but as this type of event

will likely only occur a handful of times in a drone's lifespan, the extra hassle would be minimal. Variables like the fields of transformers, branch wires, substations, etc.… could be temporarily ignored. In addition, the endless array of flight dynamics of various aircraft can be removed from the equation. This method may help prevent crashes with a much wider array of EMI sources such as street lights and construction equipment. It will also likely be much more robust as a fully automated system has many more points of failure. Its simplicity would give it broad compatibility across the market and adding it to an existing design would be as simple as mounting it on a drone, connecting the power and communication wires, and adding a few lines of code. In addition, as the hardware will be identical to a full tracking version, features can be added through paid software updates as we finish them like Tesla's business model.

The hardware required is becoming clearer at this point and will most likely consist of the following: the three axis Honeywell magnetometer (or Trifield method if our tests go well), three axis e-field sensor, physical high/low pass filters for each channel, amplifiers for each e-field axis, power conditioning, and a processor. There are many processors such as the Texas Instruments MSP430 line that have built in ADC's and communication pins. To ensure broad compatibility, it should at a minimum have I2C and SPI communications. Everything else like additional filtering, FFT analysis, and vector calculations can be done through software so the only major unknown component at this point is the electric field sensor.

## 8. Roadmap/Future Work

Tackling the shielding problem is by far my biggest concern and priority for the immediate future. Shielding is a major source of failure in robotics under normal circumstances, but our situation is just about the worst-case scenario. Our system is exposed to some of the largest fields on earth and to make matters much worse the signals we need to detect are indiscernible from the noise itself. This impacts pretty much all downstream work. We are already in the process of converting

everything to double-shielded twisted pair wiring designed specifically for high EMI environments. We will begin testing Faraday cages and various grounding techniques shortly after.

The electric field sensor design and separation of power line noise from drone noise are the other major priorities. On the electric field front, we will continue testing our free-body design and attempt a basic calibration with reference to the Trifield. I have started research into Receiver Operator Characteristic curves as a means of correctly differentiating power lines from drones. Once these steps are complete, we can do a basic ground-based avoidance demonstration with our lab prototype and then begin designing an MVP.

## 9. Bibliography


1. “Drones: Reporting for Work.” *Goldman Sachs*, www.goldmansachs.com/insights/technology-driving-innovation/drones/.
2. Hull, David M, and Ross N Adelman. *METHOD OF AUTONOMOUS POWER LINE DETECTION, AVOIDANCE, NAVIGATION, AND INSPECTION USING AERIAL CRAFTS*. 8 May 2018.
3. Adelman, Ross N, and David M Hull. “US Army Research Laboratory Power-Line UAV Modeling and Simulation (ARL-PLUMS Ver 2.x) Software Tool User Manual and Technical Report.” *US Army Research Laboratory*, 2015.
4. P. Bingham, Richard. (2001). HARMONICS - Understanding the Facts.
5. “Sensors and Actuators.” *How Magnetoresistive Sensor Works*, sensors-actuators-info.blogspot.com/2009/08/magnetoresistive-sensor.html.
6. Tumanski, Slawomir. “Induction Coil Sensors—a Review.” *Measurement Science and Technology*, vol. 18, no. 3, 19 Jan. 2007.
7. Yao, Wenxuan, et al. “Pioneer Design of Non-Contact Synchronized Measurement Devices Using Electric and Magnetic Field Sensors.” *IEEE Transactions on Smart Grid*, vol. 9, no. 6, 2018, pp. 5622–5630., doi:10.1109/tsg.2017.2692726.
8. “Converting to Logarithmic Units.” *National Instruments*, Mar. 2018, zone.ni.com/reference/en-XX/help/371361R-01/lvanlsconcepts/convert_to_log_units/.
9. “How to Use Drones for Power-Line Inspections.” Drone U™, 6 Apr. 2018, www.thedroneu.com/blog/how-to-use-drones-for-powerline-inspections/.
10. CBS/AP. “2 Workers Killed, 2 Survive 40-Foot Jump after Helicopter Hits Power Lines in New York.” CBS News, CBS Interactive, 31 Oct. 2018, www.cbsnews.com/news/helicopter-crash-beekmantown-new-york-2-killed-2-survive-40-foot-jump-after-copter-hits-power-lines/.